Modification of Hydrophilic Property of Polypropylene Films by a Parallel-Plate Nitrogen-Based Dielectric Barrier Discharge Jet

Ming-Hung Chiang, Kuo-Chi Liao, I-Min Lin, Chi-Chang Lu, Hao-Yuan Huang, Chi-Liang Kuo, and Jong-Shinn Wu

***Abstract*—Modification of the hydrophilic properties of polypropylene (PP) films has been investigated using the postdischarge region of a pulsed nitrogen-based dielectric barrier discharge under atmospheric-pressure conditions. Results show that, for the stationary PP films, the contact angle (CA) decreases dramatically from 103° (untreated) to less than 30° (treated) with a wide range of O_2/N_2 ratios ($<1\%$) and treating distances (<10 mm). In addition, the CA can still be maintained at $\sim 40°$ after 24 h of the aging test. For the nonstationary PP films, a highly hydrophilic surface can only be obtained when the PP film is placed near the jet exit with O_2/N_2 ratios of 0.06%–0.2%. Additionally, the CA can only be maintained at $\sim 80° - 90°$ when the moving speed is ~ 1 cm/s after 24 h of the aging test. These observations are explained through measured optical emission spectra and ozone concentration data, in which the metastable nitrogen plays a key role in breaking the surface chemical bounds and the UV emission (200–300) participates in the process of converting the ozone into oxygen radical. Furthermore, X-ray photoelectron spectroscopy analysis showed that the O/C ratio increases dramatically for improved hydrophilic surface and the incorporation of functional groups containing oxygen (e.g., C–O and C = O) is critical in increasing the aging time after plasma treatment.**

***Index Terms*—Atmospheric-pressure plasma (APP), dielectric barrier discharge (DBD), polypropylene (PP), quasi-pulsed.**

I. Introduction

POLYPROPYLENE (PP) film is a very useful polymer material that can be used in many applications, which include a protective film of other films, food packaging, automotive vehicles, clothing, and agriculture, among others [1]–[3]. PP film is widely used by blending it with other polymers because of its light and good mechanical properties and low processing costs [4], [5]. In spite of having many good merits, however, PP film exhibits hydrophobic characteristics because the basic repeating unit is hydrocarbon, and thus, it has a very poor wettability, adhesion, and printability [6]. For example, as it binds with a polar polymer, the problems like poor adhesion and easy detachment occur because the difference of surface free energy in the interface between the two polymers is quite large. Thus, an efficient and cost-effective method for surface modification of the PP film is strongly needed to further extend its practical application.

Due to the low-temperature resistance of PP films, many studies have applied low-pressure nonequilibrium plasma technologies to modify their surface properties [7]–[9]. However, these applications required careful sealing of the chamber and expensive vacuum equipment. In addition, several applications require atmospheric or continuous in-line processing, which further restrains the use of low-pressure discharges in these areas. This makes atmospheric-pressure plasmas (APPs) very attractive because they are free of these disadvantages. In addition, for long-term operation, the cost of the discharge gas is an important issue, which renders air or nitrogen the best choice among others. In this paper, we focus on the use of nitrogen with added trace oxygen as the major discharge gas.

In the past, most of the studies using nitrogen APPs for PP (or PE or PET) film surface modification have directly placed the test object in the discharge region [10]–[17], while relatively few have made the most of the postdischarge region. These studies have shown that the application of nitrogen-based dielectric barrier discharge (DBD) is relatively efficient in modifying the PP film from a highly hydrophobic (90.8°) into a relatively hydrophilic state (56.5°) after a short period of exposure (e.g., 3 s) in the discharge [7]. In addition, X-ray photoelectron spectroscopy (XPS) analysis has shown that the polar functional groups, such as C–O, C = O, and COO, were introduced onto the PP film surface after the atmospheric-pressure (AP) nitrogen plasma treatment and that the percent of oxygen-containing groups increased dramatically from 2.998% to 9.039% [10]. Akishev *et al.* [12] argued that the polar groups are mainly formed from the abstraction of hydrogen in the secondary carbon atom and that the formation and disappearance rate of polar groups become equilibrated. They also found that the decomposition of the C1s peak for PET C = O/N–C = O bonds appears and that the C–O/C–N bonds proportionally increase with N_2 treatment. However, there seems to be no systematic study available for the existence of the functional groups on PP films using a postdischarge region of nitrogen APPs.

To make the APP more flexible in practical applications, the postdischarge region, rather than the discharge region, should

Manuscript received January 21, 2010; revised March 4, 2010; accepted March 9, 2010. Date of publication April 26, 2010; date of current version June 9, 2010. This work was supported in part by the National Science Council of Taiwan, by the Institute of Nuclear Energy Research of Taiwan, and by the Ministry of Economic Affairs of Taiwan through Grants 96-2628-E-009-134-MY3, 98I004, and 98-EC-17-A-07-S2-0043, respectively.

M.-H. Chiang, I.-M. Lin, C.-C. Lu, H.-Y. Huang, C.-L. Kuo, and J.-S. Wu are with the Department of Mechanical Engineering, National Chiao Tung University, Hsinchu 300-10, Taiwan (e-mail: chongsin@faculty.nctu.edu.tw).

K.-C. Liao is with the Department of Bio-Industrial Mechatronics Engineering, National Taiwan University, Taipei 106-17, Taiwan.

Color versions of one or more of the figures in this paper are available online at http://ieeexplore.ieee.org.

Digital Object Identifier 10.1109/TPS.2010.2045769

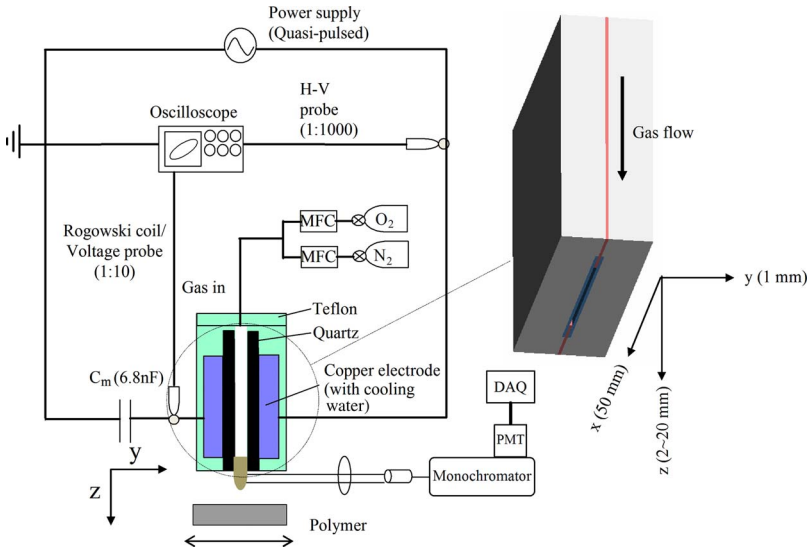

Fig. 1. Sketch of the APPJ system.

be used, although it is expected that very few charged species will be present there. The other issue is that the gap distance between electrodes is often very small (on the order of 1 mm), which further justifies the use of a postdischarge region. For thin foils, there is no problem for them to move through the small distance between electrodes. However, for the substrate with larger thickness or area, the use of the discharge region as the treatment zone may be difficult. Thus, the major goal of the present study is to investigate the efficiency of surface modification by the postdischarge region of a nitrogen-based DBD, considering the effects of several important parameters.

In this paper, we present the results of surface modification of a PP film by applying the postdischarge region of a nitrogen-based planar DBD. Effects of oxygen addition into the nitrogen DBD and treating distance between the DBD and PP film on the hydrophilic properties are investigated. Surface hydrophilic properties, roughness, and chemical composition (elements and functional groups) were measured using the contact angle (CA) machine, atomic force microscopy (AFM), and XPS, respectively. Optical emission intensity from the excited species and ozone concentration in the postdischarge region were measured using an optical emission spectrometer and an ozone analyzer, respectively, which are then used to explain the measured CAs for the stationary and nonstationary PP films.

The remainder of this paper is organized as follows: Experimental methods are introduced next, followed by the results and discussion, which include characterization of electrical properties of DBD, OES data, measurements of the ozone concentration, CA measurements (stationary and nonstationary PP films), AFM analysis, and XPS analysis. Finally, some major findings of this paper are summarized.

II. Experimental Method

The surface treatment was carried out using a dielectric nitrogen-based discharge system, as shown in Fig. 1 [18]. Fig. 1 illustrates the schematic diagram of a planar DBD atmospheric-pressure plasma jet (APPJ) along with a gas supply system and the instrumentations for electrical and optical emission spectroscopy (OES) measurements. This APPJ consists of two parallel copper electrodes (50 mm $\times$ 50 mm $\times$ 8 mm each) with embedded cooling water. Each of the electrodes was covered with a 70 mm $\times$ 70 mm $\times$ 1 mm quartz plate. Distance between the two dielectric plates (quartz) was kept at 1 mm throughout the study. This DBD assembly was driven by a quasi-pulsed bipolar power supply (Model Genius-2, EN Technologies, Inc.) at a fixed frequency of 60 kHz. The output power from the power supply was fixed at 500 W throughout the study. Input voltage and output current waveforms across the electrodes of the parallel-plate discharge were measured by a high-voltage probe (Tektronix P6015A) and a Rogowski coil (IPC CM-100-MG, Ion Physics Corporation, Inc.), respectively, through a digital oscilloscope (Tektronix TDS1012B). For the measurement of the Lissajous figure ($Q-V$ characteristics) of the discharge, a capacitor with capacitance $C_m = 6.8$ nF and a voltage probe (Tektronix P2220) were used together. Various working gases flowing between the parallel plates include N_2 (99.99% purity) and its mixture with trace oxygen (99.99% purity) with different volume fractions in the range of 0.004%–1.6%. The flow rates were controlled by manually adjustable flowmeters. Total flow rate was fixed at 50 slm throughout the study.

The optical emission spectral intensity of the APPJ in the postdischarge region was measured using a monochromator (PI Acton SP 2500) with a photomultiplier tube (Hamamatsu R928). The CAs, before and after plasma treatment, were measured using a commercial KRÛSS Easy Drop optical system (KRÛSS GmbH–Germany). In this paper, distilled water drops of 2 μL were used as the test liquid. The AFM images for measuring the roughness of the sample surface were obtained using a Veeco Dimension 5000 Scanning Probe Microscope (D5000). XPS analysis of the sample was conducted using a dedicated surface characterization spectroscopy (ESCA PHI 1600). Ozone concentration was measured using an ozone analyzer (API, Model 450), which is based on the absorption of 254 nm of UV light due to an internal electronic resonance of the O_3 molecule. In addition, the gas temperatures (measured

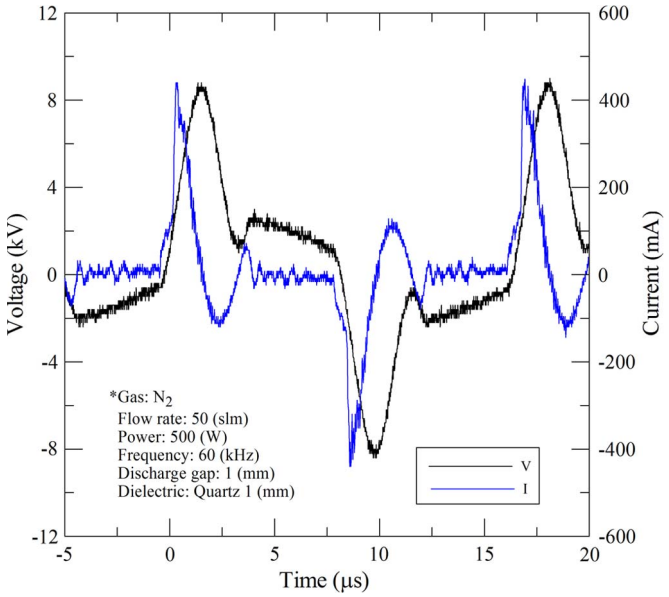

Fig. 2. Typical current and voltage waveforms for N_2 discharge.

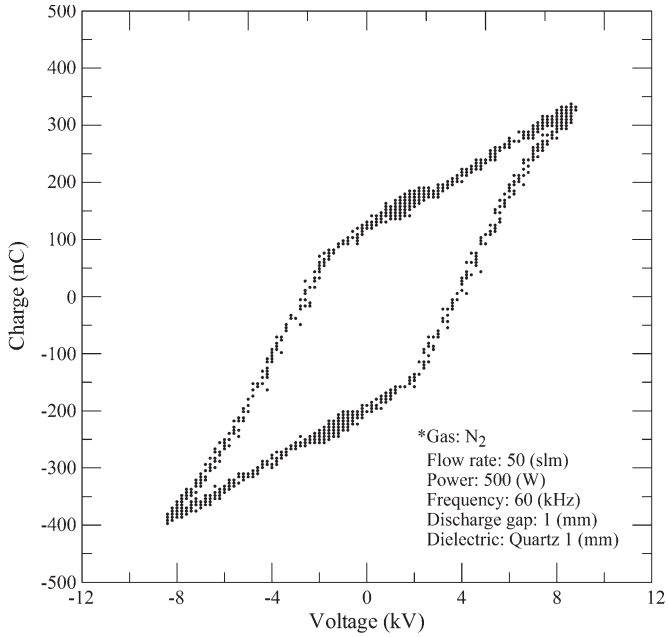

Fig. 3. Typical Lissajous figure for a parallel-plate DBD APPJ of N_2 discharge.

by a K-type thermocouple) in the jet region ($z = 2{-}20$ mm) were generally low in the range of 50 °C–80 °C under the typical operating conditions, which is considered safe for the surface modification of the PP film.

For the PP film treatment, the distance between the planar-DBD APPJ bottom edge and the PP film was varied, while the PP film (0.31 mm in thickness and density of $0.91{-}0.92$ g/cm^3, Nan-Ya, Inc.) was either stationary or transported by a preprogrammed nonstationary stage. Moving speed of the PP film was in the range of 0.5–8 cm/s throughout the study.

III. Results and Discussion

A. Electrical Characterization of the DBD

Fig. 2 shows the typical measured input voltage (60 kHz) and discharge current waveforms under the condition of 50 slm (flow rate of N_2) and 500 W (the output power from the power supply). Pulsed width is approximately 3 μs. Results show that the discharge current increases rapidly as the voltage exceeds some value ($\sim$4 kV) and decreases rapidly as voltage further increases to some level. The rapid decrease of the current is mainly due to the charge accumulation on the dielectric surface, which is a well-known mechanism of DBD to prevent the discharge from arcing. It is also interesting to observe that the current changes direction from positive to negative as the applied voltage reaches the maximal value ($\sim$8.5 kV). After the pulse, the filament current oscillates between positive and negative values at lower voltage, mainly because of the displacement current (large rate of change of applied voltage). The measured peak current for N_2 is approximately 0.4 A for 25 cm^2 of discharge area, which is equivalent to $\sim$0.016 A/cm^2 in terms of current density.

Fig. 3 shows the typical Lissajous figure obtained for the same test conditions as shown in Fig. 2. The shape of the $Q{-}V$ curve is a distorted parallelogram [19] as observed in a DBD driven by a sinusoidal ac power source. Results show that, as the voltage reaches the peak value ($\sim$8.5 kV), the maximal effective charge ($\sim$350 nC) across the electrodes is obtained, which extinguishes the discharge (zero current) caused by the shielding effect, as shown in Fig. 2. As the voltage continues to decrease, the effective charge begins to decrease as expected. The electrical energy consumed per voltage cycle E and the plasma absorbed power P can be estimated by the following relations [19]:

$$E = \oint V(t)\, dQ \equiv \text{area of } (Q{-}V) \text{ diagram} \tag{1}$$

$$P = \frac{1}{T}E = fE \tag{2}$$

where f is the frequency of the quasi-pulsed power voltage. Thus, the corresponding plasma absorbed power in this case is 175 W, and efficiency is about 35%. We have calculated the energy density [20] with the value of $4.4{-}70$ J/cm^2 with the moving speed of 0.5–8 cm/s.

B. Images of APPJ and OES Measurements of the Postdischarge Region

Fig. 4 shows the typical images of the postdischarge region for N_2 and $N_2 + 0.06\%$ O_2 discharges under the conditions of 50 slm and 500 W, which were taken after 0.2–2 s of imaging. For pure nitrogen discharge, the plume extends to a longer distance ($\sim$2.5 cm) with a yellow to orange color. It becomes even shorter ($\sim$1 cm) with a blue color with 0.06% of trace oxygen addition. These color changes can be clearly explained from the OES measurement, as typically shown in Fig. 5, which shows the optical emission spectra in the visible range obtained in the postdischarge region. It is clearly seen that, as 0.06% oxygen was added, the blue lines were greatly enhanced, which leads to the observed blue plume. In addition, it is interesting to see that, as 1.6% oxygen was added, most of the optical emissions in the visible range diminished, which leads to an invisible plume.

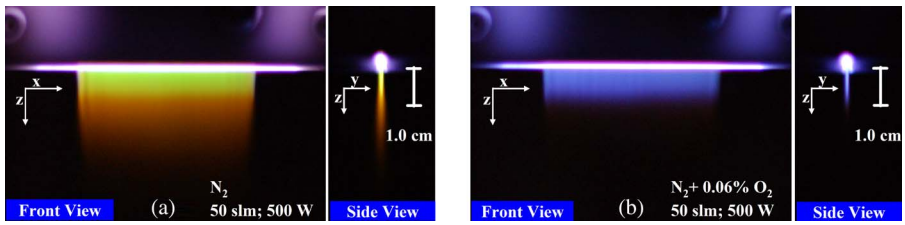

Fig. 4. Images of postdischarge region of APPJ with discharge gases consisting of (a) N_2 and (b) $N_2 + 0.06\%$ O_2.

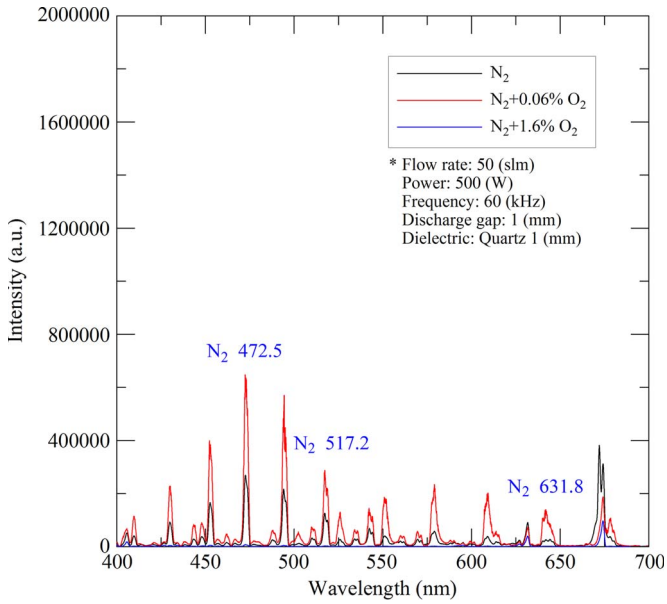

Fig. 5. OES distribution (400–700 nm) for different discharge gases of a N_2-based APPJ.

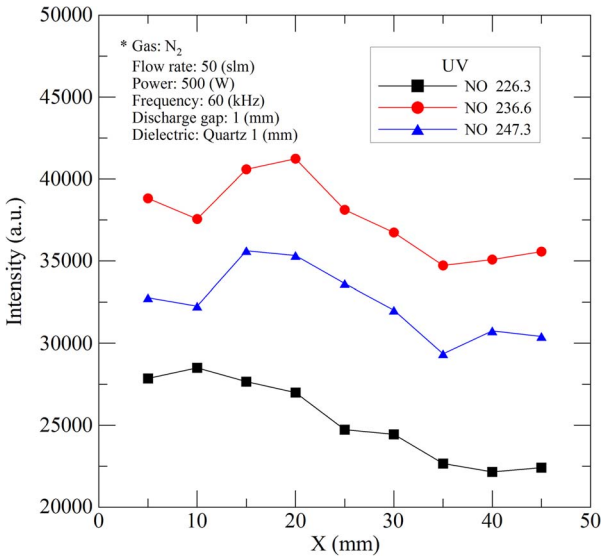

Fig. 6. UV emission intensity distribution along the channel exit (X-direction) at $z = 4$ mm for the nitrogen DBD.

Fig. 6 shows the three typical UV emission lines (226.3, 236.6, and 247.3 nm) integrated along the channel exit (X-direction) at $z = 4$ mm for the pure nitrogen DBD. These lines are typical NO-γ emissions often seen in a typical nitrogen DBD, which is attributed to the collisions between abundant metastable state nitrogen molecules $[N_2(A^3 \sum_u^+)]$ and ground

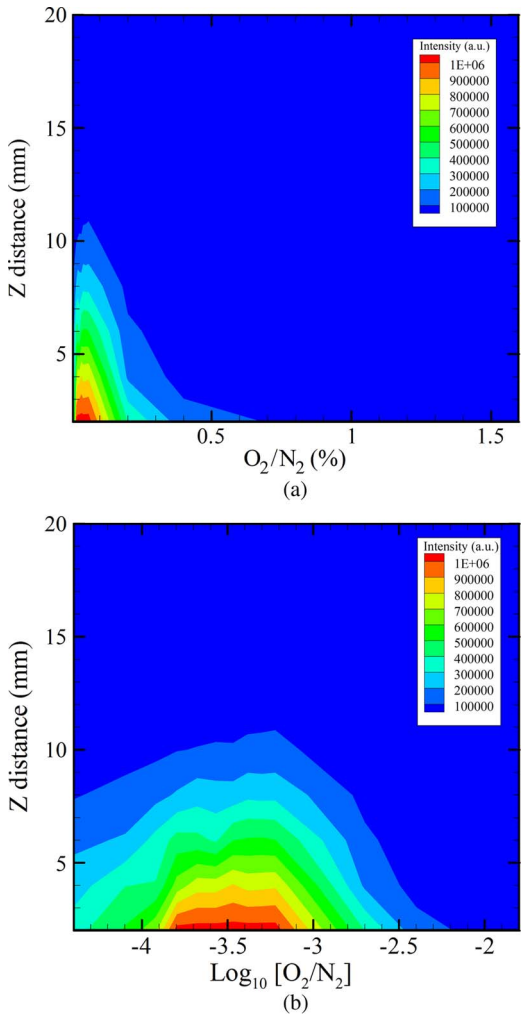

Fig. 7. OES intensity of 236.6 nm (a.u.) as a function of oxygen addition percentage and distance from the DBD exit for a N_2-based APPJ. (a) Linear scale. (b) Logarithm scale.

NO species. Results show that the intensity distribution is relatively uniform either for N_2 or $N_2 + 0.06\%$ O_2 discharges, considering the experimental uncertainties of OES measurements. This observation is important for applications which require large-area uniformity. In addition, the emission intensity of 236.6 nm is the highest among these emission lines, which is similar to some earlier observations [21]. To have a clear picture of how the UV emission intensity (e.g., 236.6 nm) varies with its position in the postdischarge region and the concentration of oxygen addition into the nitrogen discharge, we have summarized the measurements in Fig. 7. Fig. 7(a) shows that the UV emission generally increases with increasing amounts of trace oxygen addition and reaches a maximal value with only 0.06%

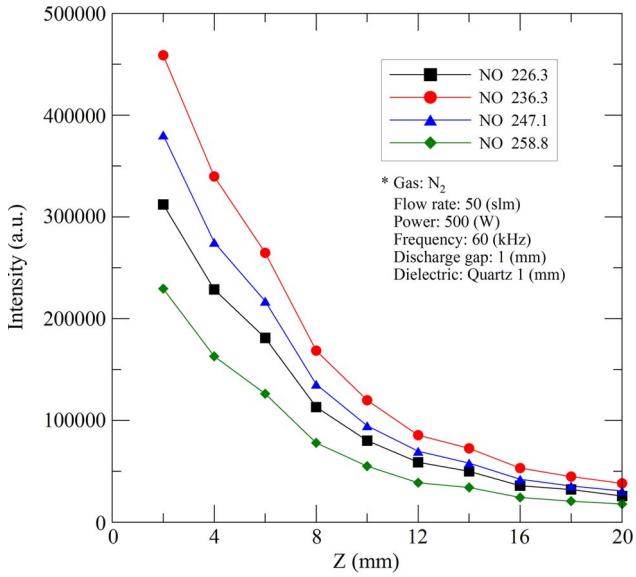

Fig. 8. Axial distribution of UV emission 200–300 nm for pure N_2.

oxygen addition. For clarity of data presentation in the cases of trace oxygen addition, results are also plotted in a logarithm scale in Fig. 7(b). Note the NO-γ emission is appreciable even with the "pure" nitrogen case, since there are always impurities (oxygen) existing in the commercial nitrogen bottle. Further addition of O_2 ($>0.06\%$) greatly reduces the UV emission, which is probably caused by the very high electron affinity of oxygen that can appreciably reduce the amount of excited nitrogen $[N_2(A^3\sum_u^+)]$. In addition, UV emission generally decreases rapidly with increasing downstream distance from the channel exit, probably because of dramatically decreasing amounts of excited nitrogen as it is quenched by entrained ambient air. These trends can also be clearly seen in Fig. 8.

C. O_3 Measurements

Fig. 9 shows the measured O_3 concentration as a function of the ratio of O_2 to N_2 at different distances from the DBD exit. Results show that ozone concentration increases from <10 ppm at $z = 2$ mm up to 30 ppm at $z = 8-10$ mm and then decreases gradually down to <20 ppm at $z = 20$ mm for $O_2/N_2(\%)$ less than 0.012%, while it increases rapidly starting at an $O_2/N_2(\%)$ larger than 0.3%–0.5% and reaches up to >220 ppm at an $O_2/N_2(\%)$ of 1.5% at $z = 8-10$ mm. The highest concentration of ozone exists as $z = 8-10$ mm at all ratios of an $O_2/N_2(\%)$ except the region between 0.016% and 0.2%. The distribution of zone concentration and the distribution of UV emission are directly correlated with the CA measurements, which will be explained shortly.

D. CA Measurements

Stationary PP Film: Fig. 10 shows the distribution of measured CAs of the PP film as functions of downstream distance ($z = 2-20$ mm) and ratio of $O_2/N_2(\%)$ (0.004%–1.6%) right after the plasma treatment. Note that the CA of the untreated sample is measured to be 103°. The results are obtained by averaging over three to five measurements over a region of

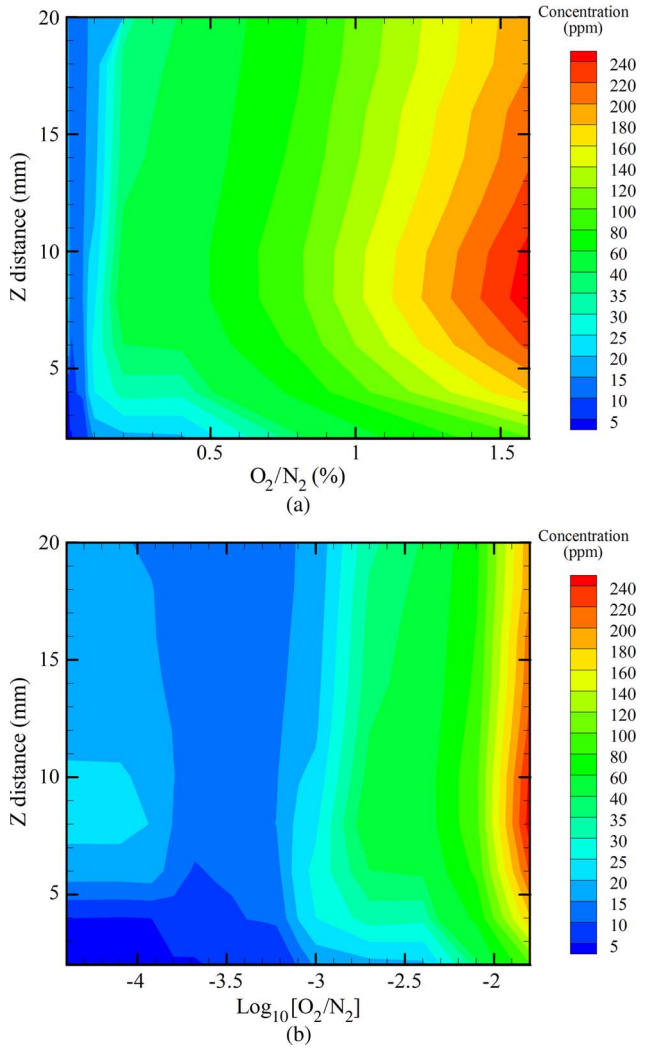

Fig. 9. Distribution of O_3 concentration as a function of distance from the DBD exit and $O_2/N_2(\%)$. (a) Linear scale. (b) Logarithm scale.

10 mm $\times$ 10 mm of a PP film with $\pm 3°$. Results indicate that the favorable operating conditions (CAs $< 30°$) include the following: 1) $z = 6-9$ mm and $O_2/N_2 < 0.008\%$; 2) $z = 2-10$ mm and $0.04\% < O_2/N_2 < 0.3\%$; and 3) $z = 0-6$ mm and $0.6\% < O_2/N_2 < 1.0\%$. The above observations can be explained by the distributions of ozone and UV emission in the near jet region. It is interesting to learn that the lowest CA (23°) occurs at the ratio of O_2/N_2 near 0.06% at $z = 2$ mm in Region 2), which is very close to the exit of the DBD. This can be attributed to the strong UV emission (200–300 nm) near this condition (Fig. 7), where the ozone can efficiently absorb and convert into an oxygen radical [21], which can easily react with the surface as will be demonstrated later. In addition, UV emission in the range of 200–300 nm can also directly play an important role in breaking the chemical bonds of C–H (4.2 eV) and C–C (3.8 eV) since, for example, the photon energy of 236.6 nm is 5.74 eV. In Region 1), the ozone concentration has a maximal value at $z = 6-9$ mm (as shown in Fig. 9) due to the entrainment of oxygen from the ambient, where the UV emission is still appreciable (as shown in Figs. 7 and 8) for the ozone to convert efficiently into an oxygen radical. In Region 2), both ozone concentration and

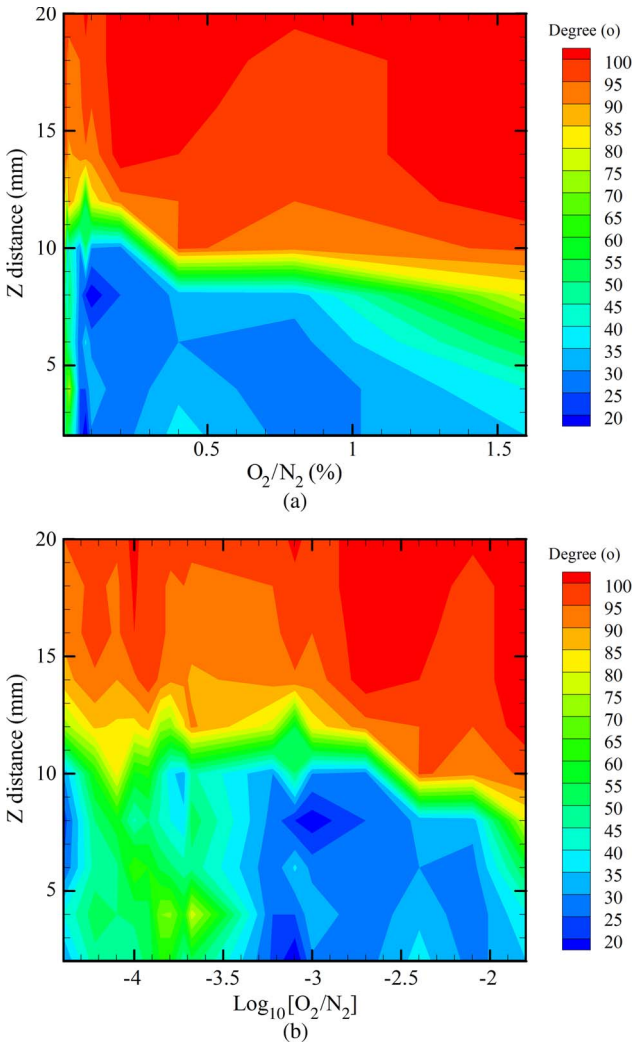

Fig. 10. Distribution of measured CAs as a function of downstream distance and ratio of $O_2/N_2(\%)$. (a) Linear scale. (b) Logarithm scale.

UV emission are appreciable, which leads to the production of a significant amount of oxygen radicals. In addition, as mentioned earlier, strong UV emission also plays an important role when the PP film is nonstationary; this will be discussed next. In Region 3), the ozone concentration is very high (40–80 ppm) (Fig. 9), although the UV emission becomes relatively low in the downstream region after $z = 10$ mm (Fig. 7).

Nonstationary PP Film: Measured CAs for nonstationary films are summarized in Tables I and II at $z = 2$ mm. Table I lists the CAs for various O_2/N_2 ratios (0%–1.6%) at a nonstationary speed of $v = 0.5$ cm/s, while Table II summarizes the data at various nonstationary speeds for the PP film (0.5–8 cm/s) for four typical O_2/N_2 ratios in which the CAs are in the range of 26°–39° as shown in Table I. Only the cases of $z = 2$ mm for the nonstationary films are presented here since we have found that the CAs become very large after this distance (e.g., $> 70°$ at $z = 4$ mm with O_2/N_2 ratio of 0.06%) because of a low residence time and very low UV emission at further downstream locations. At the distance of $z = 2$ mm, we have found that the minimal CA occurs at O_2/N_2 ratios in the range of 0.06%–0.2%. However, as the nonstationary speed increases up to $v = 1.0$ cm/s, only at the condition of O_2/N_2 ratio of 0.06% is the CA low enough (33°), while all other CAs are larger than 45°. This can be attributed to the very strong UV emissions that occur when the ratio of O_2/N_2 is between 0.02% and 0.2% near the jet exit (as shown in Fig. 7). This leads to a direct breaking of the surface chemical bounds, such as C–H (4.2 eV) and C–C (3.8 eV), without the help of oxygen radicals. Unlike the stationary film, the residence time on the surface for the conversion of the ozone into an oxygen radical (very short life time) by absorbing UV emissions (200–300 nm) becomes increasingly insufficient with the increasing nonstationary speed of the PP film. Thus, only the direct bond breaking by UV emissions can play an important role in the surface modification of nonstationary PP film. In general, the CA increases with the increasing nonstationary speed of the PP film. As the speed reaches $v = 8$ cm/s, surface modification of the PP film using a nitrogen-based DBD jet becomes effectively useless under the current operating conditions.

TABLE I
MEASURED CAS OF NONSTATIONARY PP FILM AT DIFFERENT O_2/N_2 RATIOS AFTER PLASMA TREATMENT ($z = 2$ mm AND $v = 0.5$ cm/s)

O_2/N_2 (%)	Contact angle (°)
0	75
0.002	74
0.004	73
0.006	72
0.008	70
0.01	77
0.012	77
0.014	76
0.016	74
0.019	73
0.021	73
0.06	26
0.2	27
0.4	33
0.8	39
1.6	77

TABLE II
MEASURED CONTACT ANGLES OF NONSTATIONARY PP FILM AT FOUR TYPICAL O_2/N_2 RATIOS AFTER PLASMA TREATMENT ($z = 2$ mm AND $v = 0.5$–8 cm/s)

V (cm/s)	O_2/N_2 (%)			
	0.06	0.20	0.40	0.80
0.5	26	27	33	39
1	33	45	50	72
2	80	82	94	94
4	97	91	101	98
8	100	97	103	103

E. Aging Effect

Fig. 11 shows the typical aging test within 24 h (at room temperature) of the improved hydrophilic property (CA) of stationary and nonstationary PP films after plasma treatment. Results show that, for all the cases shown in Fig. 11, the CAs are all less than 30° right after plasma treatment. However, the CAs

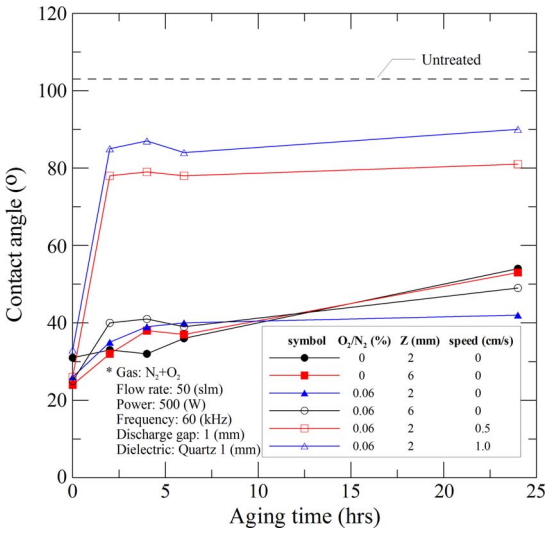

Fig. 11. CAs of water on PP film versus various gases, z-direction, and aging time were treated in the $N_2 + O_2$ DBD environment.

TABLE III
RMS ROUGHNESS OF PP FILM AT DIFFERENT TREATING DISTANCES MEASURED BY AFM

z (mm)	RMS roughness (nm)
Untreated	40.4
2	19.6
6	17.8
20	28.6

for the nonstationary PP films rise very quickly to $\sim 80^\circ$ ($v = 0.5$ cm/s) and $\sim 90^\circ$ ($v = 1.0$ cm/s) after 2 h of exposure to air and saturate until the end of the test (24 h), while the CAs for the stationary PP films increase to 5°–15° after the first 2–4 h and then saturate at $\sim 40^\circ - 50^\circ$ until the end of the test. This shows that the improved hydrophilic property, formed because of the bond breaking by the UV emission (nonstationary PP film), deteriorates quickly; however, the one caused by both the UV emission and oxygen radical (stationary PP film) can be sustained much longer. These can be further explained by the XPS analysis later.

F. AFM Analysis

Table III summarizes the typical roughness data of stationary PP film, as measured by the AFM, after treatment using the pure nitrogen discharge jet. Note that the rms roughness data were taken from a 3 μm by 3 μm section. Untreated rms roughness is 40.4 nm, but it decreases to 17.8 nm at $z = 6$ mm and gradually increases at further downstream locations (28.6 nm at $z = 20$ mm). This trend coincides with that of the measured CAs, in which a minimal value occurs in the range of $z = 6 - 8$ mm. This means that the less the roughness is, the smaller the CA is. The DBD treatments may thus produce some effects such as removal of contaminants, oligomers, and amorphous layers existing on the surface, allowing chemical activation of the material [13], but this requires further investigation to understand the underlying physics in the near future.

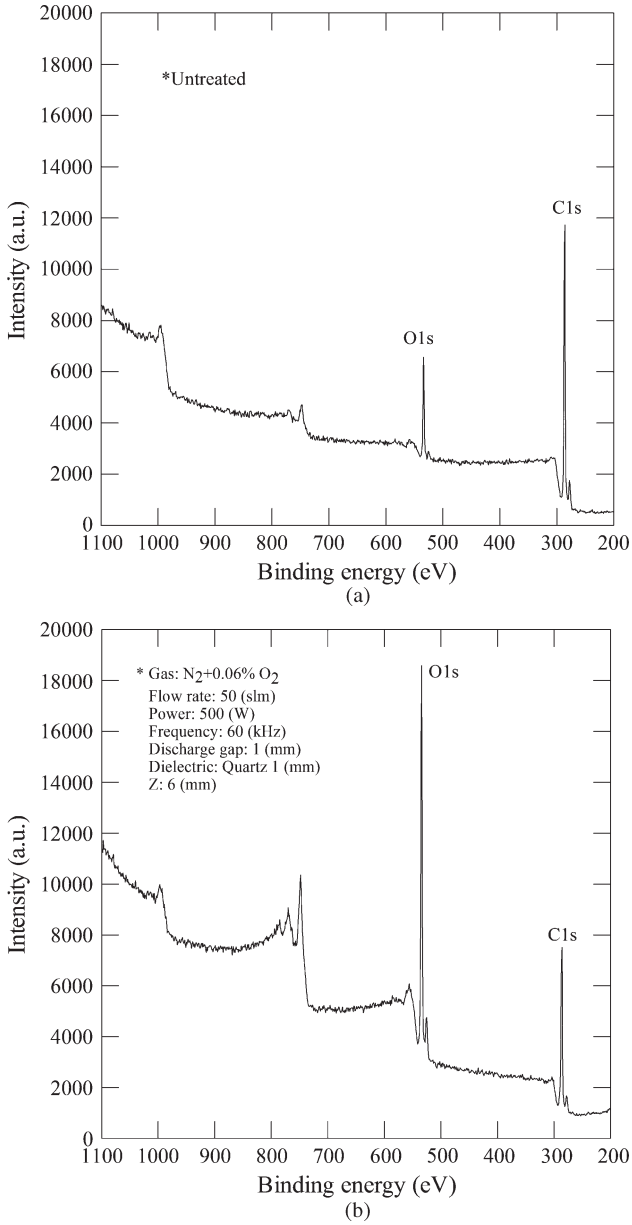

Fig. 12. XPS scan spectra of (a) untreated PP film and (b) $N_2 + 0.06\%$ O_2 treated PP at $z = 6$ mm.

G. XPS Analysis

To analyze the change of chemical compositions on the PP film surface and the chemical binding state, an XPS machine (ESCA PHI 1600, Mg anode at 250 W and 15 kV, 1253.6 eV, an electron takeoff angle of 45° with respect to the PP film surface, chamber pressure below 2×10^{-8} torr) was used. Fig. 12 shows the XPS scan spectra of untreated and treated stationary PP ($N_2 + 0.06\%$ O_2) films. After plasma treatment, the O1s peak increases dramatically, while the C1s peak decreases in a milder fashion. This means that the appreciable amount of oxygen radical has been incorporated into the surface compound, while carbon has been removed efficiently.

Table IV summarizes the corresponding quantitative atomic compositions, and the fractions of peak area of untreated and treated samples, as calculated from the C1s core level spectra on the surface of the PP film for various typical test conditions.

TABLE IV
ATOMIC PERCENT CONCENTRATION AND RATIO AND PERCENT PEAK AREA OF XPS C1s CORE LEVEL SPECTRA OF UNTREATED PP AND APP TREATED PP

O_2/N_2 (%)	z (mm)	Speed (cm/s)	Exposure time (s)	Contact angle (°)	C (%)	N (%)	O (%)	O/C	C-C / C1s (%)	C-O / C1s (%)	C=O / C1s (%)	COO / C1s (%)
0	2	0	5	35	58.1	0.5	41.4	0.7	85.3	7.6	6.9	0.1
0	6	0	5	23	58.0	0.2	41.3	0.7	88.8	4.9	5.8	0.6
0	20	0	5	95	70.8	0	29.3	0.4	96.3	3.8	0	0
0.06	2	0	5	24	53.9	1.5	44.6	0.8	88.3	8.0	3.5	0.2
0.06	6	0	5	26	52.7	0	47.3	0.9	92.7	4.2	3.1	0
0.06	20	0	5	96	67.9	0	32.2	0.5	96.2	3.8	0	0
0	2	1	0.1	87	65.0	0.5	34.6	0.5	89.2	10.8	0	0
0.06	2	1	0.1	33	62.4	0.4	37.3	0.6	95.4	4.6	0	0
untreated				103	88.9	0	11.1	0.1	97.1	2.9	0	0
untreated (ethanol)				103	83.6	0	16.4	0.2	99.9	0.1	0	0

Results show that, after plasma treatment, there is a tremendous increase of the O/C ratio at $z = 2$ and 6 mm that is found. In the stationary cases, at $z = 2$ and 6 mm, we can find large increase of O/C ratio. The reason can be possibly explained as follows. At $z = 2$ mm, ozone absorbs abundant NO-γ UV emission (200–300 nm) and produces abundant highly chemically active oxygen radicals by photo dissociation $[O_3 + h\upsilon \rightarrow O(^3P) + O_2]$ which further react with the PP film. The N_2 first positive lines $[N_2(B^3\prod_g) \rightarrow N_2(A^3\sum_u^+)]$ (500–700 nm in Fig. 5) show that abundant metastable $N_2(A^3\sum_u^+)$ (energy $= 6.2$ eV) is generated, which can be transported to the substrate by the jet stream and easily break C–C (3.8 eV) chemical bonds, which is similar to some earlier observations [22], [23]. At downstream ($z = 6$ mm), UV emission becomes weaker, but ozone becomes more abundant because of ambient entrainment, which can still produce appreciable oxygen radicals. In addition, the amount of long-lived metastable $N_2(A^3\sum_u^+)$ is still high enough to reach the PP film and break the chemical bonds of the PP film. The aforementioned two mechanisms result in tremendous O/C increase at both $z = 2$ and 6 mm. However, at further downstream position ($z = 20$ mm), no UV emission is possible, and the amount of metastable $N_2(A^3\sum_u^+)$ becomes smaller, which makes the O/C ratio increase less obvious as shown in Table IV.

For example, the O/C ratio increases from 0.1 up to 0.9 for stationary PP film at $z = 6$ mm for the condition of $N_2 + 0.06\%$ O_2, in which the measured CA is 23°. This again confirms that the polar functional groups containing oxygen were introduced on the PP film surface. By comparing the corresponding measurements of the CAs in Table IV, we can conclude that the larger the O/C ratio, the smaller the CA. Fig. 13 shows a graph by separating the peak of the samples in the C1s level through curve fitting. As shown in Fig. 13, the polar functional groups, such as C–O (286.8 eV), C = O (287.8 eV), and COO (289.7 eV), were introduced on the PP film surface after an AP nitrogen plasma treatment, although the fraction of COO is very small and less than the experimental uncertainties. Nevertheless, these can only be considered qualitative only since they were fitted values. Results show that the greater the amount of functional groups C–O and C = O there is, the better the hydrophilic property of the PP film is. In addition, the appearance of the C = O group may also explain the longer measured aging time for stationary film cases as found earlier (Fig. 11), probably because of the higher binding energy as compared to that of C–O. As the trace oxygen is added into the nitrogen ($O_2/N_2 = 0.06\%$), more ozone is generated [Fig. 7(a)] and more UV (200–300 nm) is emitted (Fig. 5) which produces more abundant oxygen radicals to react with the PP film. This can be confirmed by the increase of the O/C ratio (0.8–0.9) as compared to the pure nitrogen case (0.7) in Table IV and thus results in better hydrophilic property at $z =$ 2 mm. At $z = 6$ mm, much lower UV emission causes the role of this mechanism less important than the metastable nitrogen, as can be seen from almost the same CA (23° versus 26°).

Based on this observation, how to efficiently incorporate C = O and even COO functional groups, which have higher binding energies, may become an important issue for longer aging time and should be subject to further investigation.

IV. CONCLUSION

Modification of the surface hydrophilic properties of PP films has been presented in this paper using the postdischarge region of a pulsed nitrogen-based DBD under AP condition. The discharge system was first characterized by measurements of electrical and optical properties, and ozone concentration in the jet region. The DBD jet was then applied to treat the PP film under stationary and nonstationary conditions with various O_2/N_2 ratios ranging from 0% to 1.6% at different treating distances in the range of 2–20 mm. Results show that, for stationary PP films, the surface hydrophilic property improves dramatically from 103° (untreated) to a value less than 30° (treated) for CAs with a wide range of O_2/N_2 ratios (<1%) and

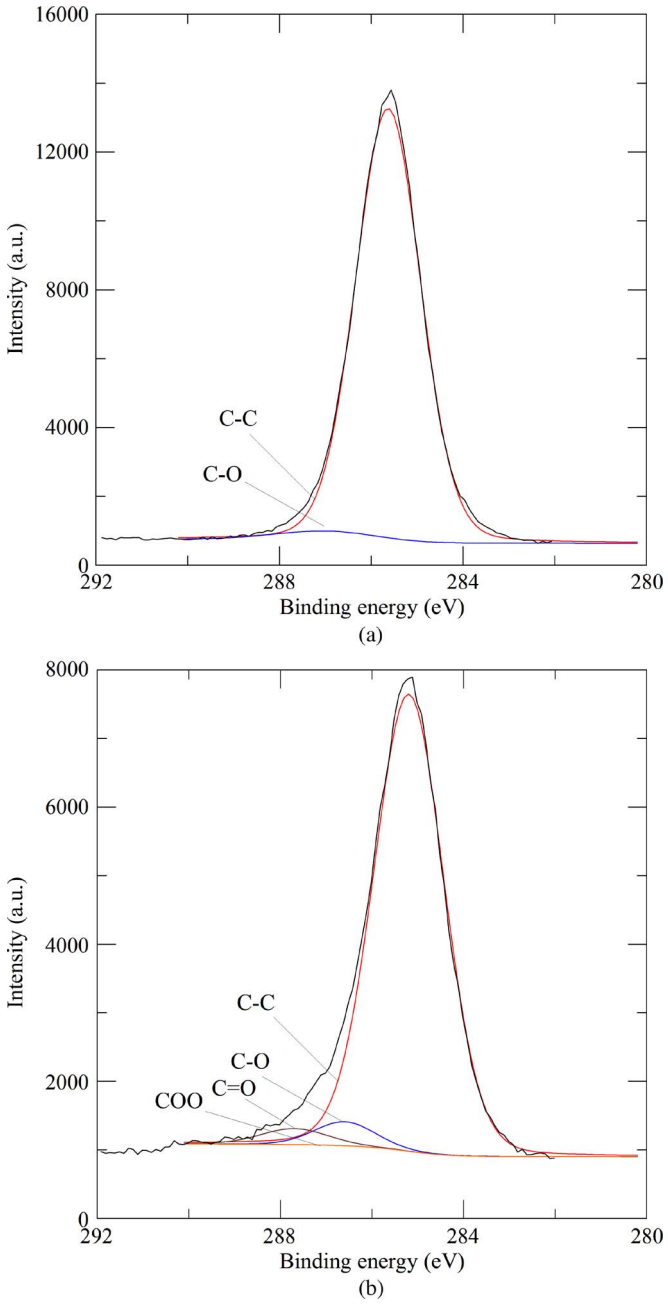

Fig. 13. C1s spectra of (a) untreated PP film and (b) $N_2 + 0.06\%$ O_2 treated PP at $z = 6$ mm.

treating distances (<10 mm). For the nonstationary PP films, highly hydrophilic surfaces can only be obtained when the PP film is placed near the jet exit (treating distance of 2–4 mm) with an O_2/N_2 ratio of 0.06%–0.2%. These observations are explained through measured optical emission spectra and ozone concentration data, in which the metastable nitrogen plays a key role in breaking the surface chemical bounds and UV emission (200–300 nm) participates in the process of converting the ozone into oxygen radical. Aging tests show that, for stationary PP films, the CA can still be maintained at $\sim 40^\circ$ after 24 h, while for the nonstationary test cases, it can only be maintained at $\sim 80^\circ - 90^\circ$ when the nonstationary speed is near 1 cm/s. By AFM analysis, we also observed that the less the surface roughness is, the smaller the CA is. Finally, XPS analysis shows that O/C ratio increases dramatically which results from the incorporation of several polar functional groups containing oxygen into the surface of PP films during plasma treatment. The greater the amount of functional groups C–O and C = O, the better the hydrophilic property of the PP film. In addition, the number of polar functional groups, such as C = O, having higher binding energy can directly influence the aging time of the hydrophilic property of PP film after the plasma treatment.

REFERENCES

[1] M. Strobel, V. Jones, C. S. Lyons, M. Ulsh, M. J. Kushner, R. Dorai, and M. C. Branch, "A comparison of corona-treated and flame-treated polypropylene films," *Plasmas Polym.*, vol. 8, no. 1, pp. 61–95, Mar. 2003.

[2] N. Y. Cui and N. M. D. Brown, "Modification of the surface properties of a polypropylene film using an air dielectric barrier discharge plasma," *Appl. Surf. Sci.*, vol. 189, no. 1/2, pp. 31–38, Apr. 2002.

[3] C. Riccardi, R. Barni, E. Selli, G. Mazzone, M. R. Massafra, B. Marcandalli, and G. Poletti, "Surface modification of poly(ethylene terephthalate) fibers induced by radio frequency air plasma treatment," *Appl. Surf. Sci.*, vol. 211, no. 1–4, pp. 386–397, Apr. 2003.

[4] D. L. Cho, K. H. Shin, W. J. Lee, and D. H. Kim, "Improvement of paint adhesion to a polypropylene bumper by plasma treatment," *J. Adhes. Sci. Technol.*, vol. 15, no. 6, pp. 653–664, 2001.

[5] F. Poncin-Epaillard, B. Chevet, and J. C. Brosse, "Reactivity of a polypropylene surface-modified in a nitrogen plasma," *J. Adhes. Sci. Technol.*, vol. 8, no. 4, pp. 455–468, 1994.

[6] M. Zenkiewicz, "Wettability and surface free energy of corona-treated biaxially-oriented polypropylene film," *J. Adhes. Sci. Technol.*, vol. 15, no. 14, pp. 1769–1785, 2001.

[7] R. Morent, N. De Geyter, L. Gengembre, C. Leys, E. Payen, S. Van Vlierberghe, and E. Schacht, "Surface treatment of a polypropylene film with a nitrogen DBD at medium pressure," *Eur. Phys. J. Appl. Phys.*, vol. 43, no. 3, pp. 289–294, Sep. 2008.

[8] S. Bhowmik, P. K. Ghosh, and S. Ray, "Surface modification of HDPE and PP by mechanical polishing and DC glow discharge and their adhesive joining to steel," *Appl. Polym. Sci.*, vol. 80, no. 8, pp. 1140–1149, May 2001.

[9] F. Ponic-Epaillard, B. Chevet, and J. C. Brosse, "Modification of isotactic poly(propylene) with a nitrogen plasma; differences in comparison to the treatment with a carbon dioxide plasma," *Markromol. Chem.*, vol. 192, no. 7, pp. 1589–1599, Jul. 1991.

[10] O. J. Kwon, S. Tang, S. W. Myung, N. Lu, and H. S. Choi, "Surface characteristics of polypropylene film treated by an atmospheric pressure plasma," *Surf. Coat. Technol.*, vol. 192, no. 1, pp. 1–10, Mar. 2005.

[11] K. Wang, J. Li, C. S. Ren, D. Z. Wang, and Y. N. Wang, "Surface modification of polyethylene films using dielectric barrier discharge plasma at atmospheric pressure," *Plasma Sci. Technol.*, vol. 10, no. 4, pp. 433–437, Aug. 2008.

[12] Y. Akishev, M. Grushin, N. Dyatko, I. Kochetov, A. Napartovich, N. Trushkin, T. M. Duc, and S. Descours, "Studies on cold plasma-polymer surface interaction by example of PP- and PET-films," *J. Phys. D, Appl. Phys.*, vol. 41, no. 23, p. 235 203, Dec. 2008.

[13] G. Borcia, G. A. Chiper, and I. Rusu, "Using a He + N_2 dielectric barrier discharge for the modification of polymer surface properties," *Plasma Sources Sci. Technol.*, vol. 15, no. 4, pp. 849–857, Nov. 2006.

[14] C. P. Klages and A. Grishin, "Quantitative ATR FT-IR analysis of chemically derivatized plasma-modified polymers surfaces," *Plasma Process. Polym.*, vol. 5, no. 4, pp. 359–367, Jun. 2008.

[15] R. Dorai and M. J. Kushner, "A model for plasma modification of polypropylene using atmospheric pressure discharges," *J. Phys. D, Appl. Phys.*, vol. 36, no. 6, pp. 666–685, Mar. 2003.

[16] C. Sarra-Bournet, G. Ayotte, S. Turgeon, F. Massines, and G. Laroche, "Effects of chemical composition and the addition of H_2 in a N_2 atmospheric pressure dielectric barrier discharge on polymer surface functionalization," *Langmuir*, vol. 25, no. 16, pp. 9432–9440, Aug. 2009.

[17] M. J. Shenton, G. C. Stevens, N. P. Wright, and X. Duan, "Chemical-surface modification of polymers using atmospheric pressure nonequilibrium plasmas and comparisons with vacuum plasmas," *J. Polym. Sci. A, Polym. Chem.*, vol. 40, no. 1, pp. 95–109, Jan. 2002.

[18] M. H. Chiang, J. Y. Wu, Y. H. Li, and J. S. Wu, "Inactivation of E. coli and B. subtilis using a quasi-pulsed power driven air atmospheric pressure plasma jet," in *Proc. Taiwan-Jpn. Symp. Appl. Plasma Bio-Med. Eng.*, Taipei, Taiwan, 2008, pp. 36–45.

[19] H. E. Wagner, R. Brandenburg, K. V. Kozlov, A. Sonnenfeld, P. Michel, and J. F. Behnke, "The barrier discharge: Basic properties and applications to surface treatment," *Vacuum*, vol. 71, no. 3, pp. 417–436, May 2003.
[20] S. Guimond and M. R. Wertheimer, "Surface degradation and hydrophobic recovery of polyoefins treated by air corona and nitrogen atmospheric pressure glow discharge," *J. Appl. Polym. Sci.*, vol. 94, no. 3, pp. 1291–1303, Nov. 2004.
[21] M. Iwasaki, K. Takeda, M. Ito, T. Yara, T. Uehara, and M. Hori, "Effect of low level O_2 addition to N_2 on surface cleaning by nonequilibrium atmospheric-pressure pulsed remote plasma," *Jpn. J. Appl. Phys.*, vol. 46, no. 23, pp. L540–L542, 2007.
[22] J. T. Herron, "Evaluated chemical kinetics data for reaction of $N(^2D)$, $N(^2P)$, and $N_2(A^3\Sigma_u^+)$ in the gas phase," *J. Phys. Chem. Ref. Data*, vol. 28, no. 5, pp. 1453–1483, 1999.
[23] C. P. Klages and A. Grishin, "Plasma amination of low-density polyethylene by DBD afterglows at atmospheric pressure," *Plasma Process. Polym.*, vol. 5, no. 4, pp. 368–376, Jun. 2008.

Ming-Hung Chiang received the M.S. degree in mechanical engineering from the National Sun Yat-Sen University, Kaohsiung, Taiwan, in 1996. He is currently working toward the Ph.D. degree with the Department of Mechanical Engineering, National Chao Tung University, Hsinchu, Taiwan.

His research interests include atmospheric-pressure plasmas, radio-frequency glow discharge, dielectric barrier discharge, plasma jets, and their applications.

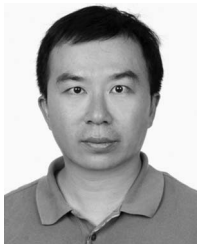

Kuo-Chi Liao received the M.S. and Ph.D. degrees in mechanical engineering from the University of Michigan, Ann Arbor, in 1992 and 1996, respectively.

He is currently an Assistant Professor with the Department of Bio-Industrial Mechatronics Engineering, National Taiwan University, Taipei, Taiwan. His research interests include precision manufacturing, crystalline plasticity, fatigue failure, and plasma applications, particularly in materials processing.

I-Min Lin received the B.S. degree in mechanical engineering from Tatung University, Taipei, Taiwan, in 2007 and the M.S. degree in mechanical engineering from the National Chiao Tung University, Hsinchu, Taiwan, in 2009.

He is currently a Research Assistant with the Department of Mechanical Engineering, National Chiao Tung University. His research interests include polymer surface treatment and property analysis of atmospheric-pressure plasma.

Chi-Chang Lu received the B.S. degree in mechanical engineering from Chang Gung University, Taoyuan, Taiwan. He is currently working toward the M.S. degree with the Department of Mechanical Engineering, National Chiao Tung University, Hsinchu, Taiwan.

His research interests include the electrical and optical diagnostics of an atmospheric-pressure plasma jet and applications of thin-film deposition.

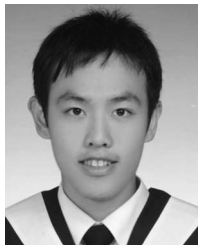

Hao-Yuan Huang received the B.S. degree in mechanical engineering from the National Changhua University of Education, Changhua, Taiwan. He is currently working toward the M.S. degree with the Department of Mechanical Engineering, National Chiao Tung University, Hsinchu, Taiwan.

His research interests include optical and electrical properties of an atmospheric-pressure plasma jet and its applications to biocompatible materials.

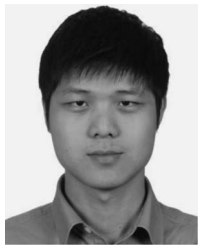

Chi-Liang Kuo received the B.S. degree in chemistry from Chung Yuan Christian University, Chungli, Taiwan, in 2003 and the Ph.D. degree in chemistry from the National Tsing Hua University, Hsinchu, Taiwan, in 2008.

He is currently a Postdoctoral Researcher with the Department of Mechanical Engineering, National Chiao Tung University, Hsinchu. His research interests include atmospheric-pressure plasma jet and its applications to thin-film deposition and surface modification.

Jong-Shinn Wu received the M.S. degree in mechanical engineering from the National Taiwan University, Taipei, Taiwan, in 1988 and the Ph.D. degree in aerospace engineering from the University of Michigan, Ann Arbor, in 1994.

He is currently a Professor with the Department of Mechanical Engineering, National Chiao Tung University, Hsinchu, Taiwan. His research interests include hybrid rocket system, low-temperature plasma physics and applications, rarefied gas dynamics simulation, advanced kinetic-based numerical method, and large-scale parallel scientific computing. He is currently an Associate Editor of the *International Journal of Plasma Science and Engineering*.